EcoMat

WILEY

EcoMat FUNCTIONAL MATERIALS FOR GREEN ENERGY AND ENVIRONMENT

RESEARCH ARTICLE OPEN ACCESS

Electrostatically Self-Powered Intelligent Force Sensor With Tunable Performance via Mechanically Guided 3D Morphing

Dongik Kam[1] | Dayeon Jang[1] | Hee Jae Hwang[2] | Sunmin Jang[1] | Sumin Cho[1] | Donghan Lee[1] | Donghyeon Yoo[3] | Junsang Yoon[4] | Seong Jin Lee[4] | Jongwoo Kim[4] | Kyoung Je Cha[5] | Dongwhi Choi[1]

[1]Department of Mechanical Engineering (Integrated Engineering Program), Kyung Hee University, Yongin, Gyeonggi, Republic of Korea | [2]School of Mechanical System Engineering, Kumoh National Institute of Technology, Gumi-si, Gyeongsangbuk-do, Republic of Korea | [3]Department of Mechanical Science and Engineering, University of Illinois at Urbana-Champaign, Urbana, Illinois, USA | [4]Department of Mechanical Engineering, Kyung Hee University, Yongin, Gyeonggi, Republic of Korea | [5]Advanced Mobility & Robot Components Group, Korea Institute of Industrial Technology, Daegu, Republic of Korea

Correspondence: Kyoung Je Cha (kjcha@kitech.re.kr) | Dongwhi Choi (dongwhi.choi@khu.ac.kr)

Received: 23 October 2025 | **Revised:** 3 December 2025 | **Accepted:** 18 January 2026

Keywords: electret | electrostatic induction | mechano-guided geometrical adaptation | self-powered sensor | tunable sensing performance

ABSTRACT

Sensors that capture diverse environmental information are crucial in the elemental technology driving the Fourth Industrial Revolution. However, the trade-off between sensitivity and working range exhibited by conventional sensors results in limitations when the target stimuli deviate from their predesigned specifications. Thus, single sensors with adjustable performance characteristics must be developed to satisfy functionality requirements in diverse environments. In this study, a Tunable Usability-Nourished Electrostatic-based self-powered force sensor (TUNE sensor) is introduced to overcome the limitations of the fixed detection performance of a single sensor. The tunable sensing performance of the TUNE sensor is achieved via mechano-guided geometrical adaptation of its three-dimensional (3D) structure formed via mechanical buckling. Continuous and reversible shape changes in the 3D structure allow modulation of the stiffness of the TUNE sensor, resulting in tunable sensing performance (sensitivity of 0.53~1.08 nC/N and working range of 1.01~0.35 N). The effectiveness of the tunable sensing performance is demonstrated through its implementation in a reconfigurable electronic scale and robotic sensing. This mechano-guided geometrical adaptation strategy offers the potential for extending the use of sensors in multivariate environments and providing new opportunities for intelligent sensing systems in various applications.

1 | Introduction

Elemental technologies, such as big data, artificial intelligence, and the Internet of Things, drive the Fourth Industrial Revolution and pave the way for an intelligent world. Because these technologies require considerable amounts of information, sensors that acquire diverse external data from the surrounding environment are essential for the Fourth Industrial Revolution [1–4]. Mechanical sensors that detect mechanical loads, including force, pressure, and strain, have been successfully applied in various fields, such as wearable electronics, health monitoring, robotics, and human-machine interfaces [5–16].

The performance of a mechanical sensor is determined by its mechanical, geometrical, and morphological properties [17–20]. Because most mechanical sensors possess unalterable properties,

Dongik Kam and Dayeon Jang contributed equally to this work.

key performance metrics such as sensitivity and working range are impossible to modify after fabrication. In particular, the sensitivity and working range of a single sensor inherently exhibit a trade-off [21]. Hence, if the target stimulus deviates from the designed performance range of a single sensor, precise measurement may become challenging or observation may even be infeasible in some cases. Therefore, the demand for sensors capable of operating in various environments necessitates the development of devices with tunable properties [22–27]. This tunability enables the sensor to achieve the desired performance, tailored to specific application requirements.

Physical intelligence, which encodes capabilities such as control, actuation, adaptation, and memory into devices, has recently emerged as an important research area [28]. Among these capabilities, "adaptation", which allows a device to adjust to multilateral factors, is achieved via structural design, mechanisms, and functional materials. Representative examples include a medical robot with shape reconfigurability that can navigate through complex and narrow pathways and a chameleon-inspired camouflage robot that uses thermochromic liquid crystals to match its color to that of its surroundings [29, 30]. This exploration of adaptation helps in developing devices suitable for intellectualization. Consequently, research on the adaptability of mechanical sensors, which play a key role in the Fourth Industrial Revolution, is essential for expanding their range of applications.

In this study, we propose a Tunable Usability-Nourished Electrostatic-based self-powered force sensor (TUNE sensor) that alters its geometry to adjust its sensitivity and working range as required. The TUNE sensor utilizes a three-dimensional (3D) structure formed through a mechanically guided geometry transformation based on buckling. The mechano-guided geometrical adaptation of the 3D structure reversibly controls its shape and stiffness, imparting tunability to the sensing performance of the device. The TUNE sensor operates in a self-powered manner via force-to-charge transduction using an electret, which is a polymeric material with embedded electrostatic charges. The mechanical behavior of the 3D structure is dimensionally analyzed to provide intuitive design considerations. The potential of the TUNE sensor with tunable sensing performance is successfully demonstrated through an on-demand adjustable electronic scale. The mechano-guided geometrical adaptation approach lays the foundation for intelligent sensing systems for e-skin, the Internet of Things, and robotics.

2 | Results and Discussion

2.1 | Mechanically Reconfigurable 3D Structure Design for TUNE Sensor

The tunability of the sensing performance of the TUNE sensor is accomplished using a mechanically guided geometry transformation process that creates a complex 3D structure from a two-dimensional (2D) planar structure. After fabricating a 2D precursor consisting of polyimide (PI), an electrode, and an electret, the prepared 2D precursor is selectively attached to a biaxially prestrained elastomer (Figure 1a). Then, as the prestrain ($\varepsilon_{pre} = 0.5$) applied to the elastomeric substrate is released, and compressive force by elastomer is transmitted to the 2D precursor. Mechanical buckling occurs in the 2D precursor owing to the compressive force, resulting in a 3D structure (Figure 1b). The inset in Figure 1b shows an image of the TUNE sensor with a table-like 3D structure. Here, the table-like shape is designed to allow the structural degrees of freedom to move up and down as much as possible, because the TUNE sensor focuses on normal force. The electret used to fabricate the sensor is a polymer with artificially injected negative charges (Figure S1 in Supporting Information), which provides the sensor with a self-powered function by generating charge transfer between the two electrodes. Therefore, when a force is applied perpendicular to the 3D structure, an electrical signal corresponding to it is generated (Figure 1b).

The mechanically guided geometry transformation utilized to fabricate the TUNE sensor facilitates the manufacture of complex 3D structures and has recently been used to develop electronic devices based on them [31–39]. This is attributed to the unique functions that 3D structures provide to electronic devices such as energy harvesters and sensors. Interestingly, the shape of the 3D structure configured using this fabrication method could be reversibly reconfigured depending on the strain applied to or released from the elastomer substrate. The structural reversibility of the 3D structure allows the TUNE sensor to modulate its sensing performance, such as sensitivity and working range. Figure 1c shows the geometry transformation process of the mechano-guided geometrical adaptation and the corresponding finite element analysis (FEA) of the table-like 3D structure depending on the strain of the elastomeric substrate. After the TUNE sensor with a fully popped-up 3D structure is manufactured, the compressive force acting on the structure is gradually released when tensile strain is applied to the elastomer substrate. This mechanical trigger allows the 3D structure to recover its original 2D configuration before buckling. Conversely, upon releasing the applied strain, the compressive state is reintroduced, thereby restoring the buckled 3D structure of the TUNE sensor. These geometry transformations occur within the elastic limit of PI, ensuring continuous and reversible shape changes. It is worth noting that the extent of strain is related to the height of the table-like 3D structure and the angle of its leg. To further explain this geometrical reconfiguration of the TUNE sensor, a numerical simulation (FEA) is performed. The simulation results successfully predict the shape transformation, confirming the reliability of the mechanically guided design strategy (Figure 1c(iii)).

The mechano-guided geometrical adaptation imparts sensing performance tunability to the TUNE sensor by affecting the stiffness of the sensor device. The stiffness modulation based on the geometrical change could be explained by the decomposition of the external load applied to the 3D structure. When a load (P) is exerted on the TUNE sensor (Figure 1b), P is equally distributed on each leg of the table-like 3D structure ($P = 4P_{leg}$, where P_{leg} is the load for a single leg). Considering P_{leg} as shown in Figure S2, P_{leg} is decomposed into the components of force perpendicular ($P_{\perp leg}$) and parallel ($P_{\| leg}$) to the leg, which has the following relationship with the angle between the leg and ground (θ):

$$P_{\perp leg} = P_{leg} \cos\theta \tag{1}$$

$$P_{\| leg} = P_{leg} \sin\theta \tag{2}$$

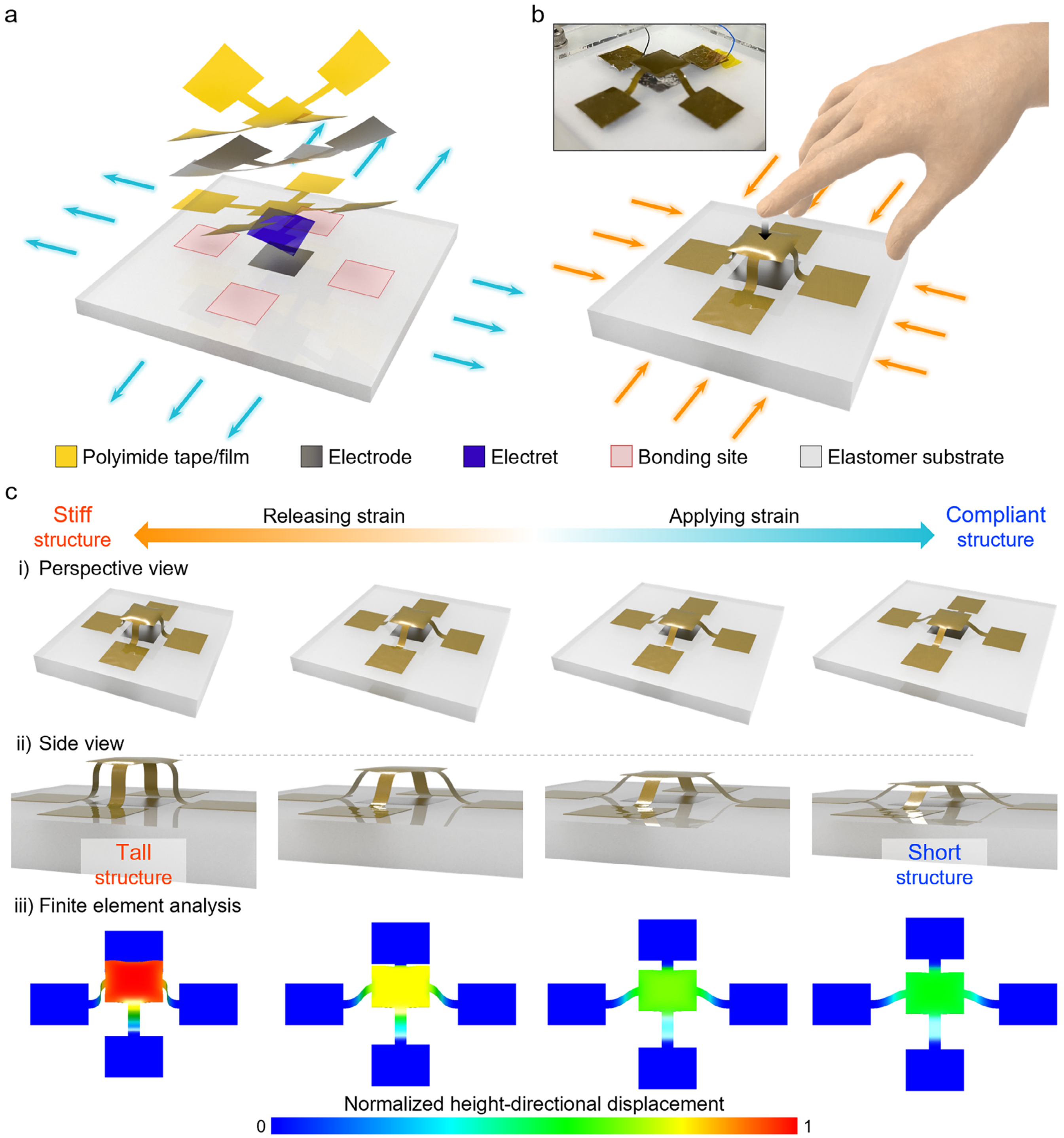

FIGURE 1 | Mechano-guided geometrical adaptation of the 3D structure of the TUNE sensor. (a) Selective bonding of the 2D precursor onto the prestrained elastomeric substrate before the mechanically guided geometry transformation process. (b) Fabrication of the TUNE sensor via mechanically guided geometry transformation. Buckling is induced by the compressive force generated from releasing the prestrain of the substrate. The inset shows the actual image of the fabricated TUNE sensor. (c) Schematic illustration and FEA of the mechano-guided geometrical adaptation of the 3D structure of the TUNE sensor. Mechano-guided geometrical adaptation by applying and releasing strain on the substrate controls the stiffness and height of the 3D structure.

In particular, $P_{\perp leg}$ induces bending of the leg, which displaces the central part of the 3D structure. According to Equation (1), $P_{\perp leg}$ increases with θ, implying that under the same loading condition, the displacement of the central part depends on the 3D structural shape. Therefore, the stiffness of the sensor device can be controlled using mechano-guided geometrical adaptation. Therefore, as the strain on the substrate is released, the popped-up 3D structure stiffens. In contrast, applying strain to the elastomer allows the structure to have compliant characteristics.

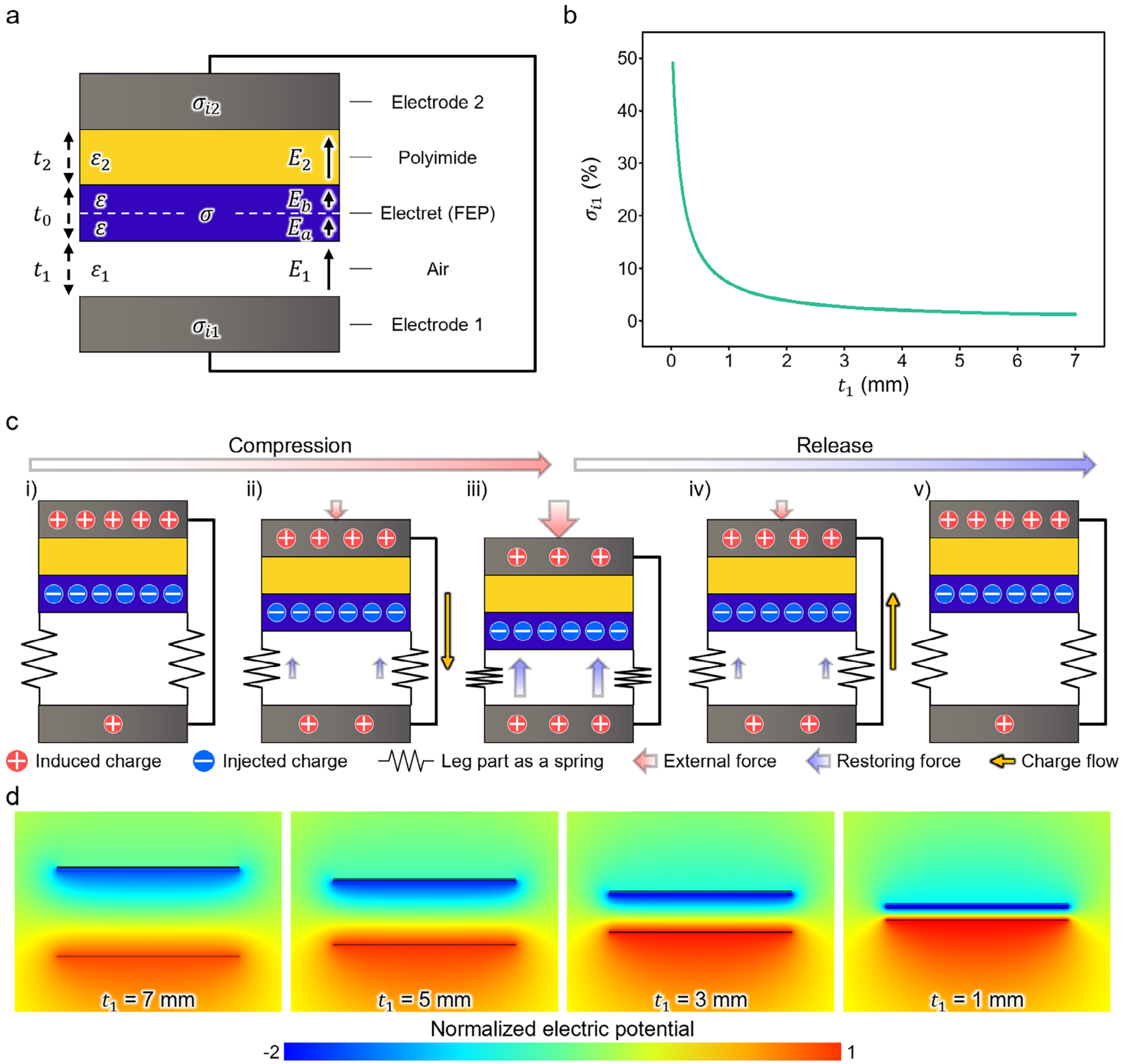

FIGURE 2 | Self-powered sensing mechanism of the TUNE sensor. (a) Schematic illustration of the central part of the TUNE sensor with the integrated electret. (b) Theoretical induced charge on electrode 1 as a function of air gap distance. (c) Self-powered sensing mechanism based on the electrostatic induction. The leg parts of the TUNE sensor act as springs and are represented simply as a spring mark. (d) Numerical simulation for the electric potential distribution in the central part of the TUNE sensor.

Consequently, the mechano-guided geometrical adaptation enables continuous and reversible modulation from stiff-tall to compliant-short properties by controlling the 3D configuration of the table-like structure. Such structural reconfigurability could become a foundational mechanism for tuning the sensitivity and working range of the TUNE sensor.

2.2 | Electrostatic Charge-Driven Sensing Mechanism of TUNE Sensor

As described above, the proposed TUNE sensor outputs an electrical signal via an electrostatic charge within the electret when force is applied. To explain the transduction mechanism between the force and electrical signals by the electret, the central part containing the electret, excluding the leg parts of the TUNE sensor, is shown in Figure 2a. According to Gauss's law and Kirchhoff's second law, the amount of positive charge induced in electrodes 1 and 2 that make up this device can be expressed as [40–42]:

$$\sigma_{i1} = \frac{\frac{t_0}{2\varepsilon} + \frac{t_2}{\varepsilon_2}}{\frac{t_0}{\varepsilon} + \frac{t_1}{\varepsilon_1} + \frac{t_2}{\varepsilon_2}}\sigma \tag{3}$$

$$\sigma_{i2} = \frac{\frac{t_0}{2\varepsilon} + \frac{t_1}{\varepsilon_1}}{\frac{t_0}{\varepsilon} + \frac{t_1}{\varepsilon_1} + \frac{t_2}{\varepsilon_2}}\sigma \tag{4}$$

The detailed derivation of Equations (3) and (4) is presented in Supplementary Note N1 (Supporting Information). Here, σ is the amount of negative charge inserted into the electret; t_0, t_1, and t_2 represent the thickness of the electret, air gap distance, and the thickness of the PI, respectively; and ε, ε_1, and ε_2 are the dielectric constants of fluorinated ethylene propylene (FEP, raw material of the electret), air, and PI, respectively. As shown by Equations (3) and (4), the amount of positive charge induced in each electrode depends on t_1 because the remaining parameters are constant in a single device. Additionally, summing Equations (3) and (4) confirms that the amount of positive charge induced into electrode 1 and the amount of positive charge flowing out of electrode 2 are the same. Therefore, the amount of charge induced in electrode 1, which depends on the displacement of the upper part containing the electret, follows the theoretical trend shown in Figure 2b. Furthermore, considering the sensing mechanism of the TUNE sensor, the amount of charge within the electret, which is influenced by the raw material, determines the amount of positive charge induced in the electrode by the electret [40]. Therefore, the greater the charge within the electret, the higher the output of the TUNE sensor at the same force, resulting in high sensitivity. FEP, used in this study, was selected because it has superior surface potential, a measure of the amount of charge within the electret, compared to other raw materials (Figure S3).

A schematic of the sensing mechanism of the TUNE sensor based on electrostatic induction is shown in Figure 2c. When an external force is applied to the TUNE sensor, the positive charges distributed on the upper electrode move to the lower electrode to maintain electrostatic equilibrium in the device (Figure 2c(i–iii)). Upon releasing the force applied to the TUNE sensor, the electret recovers its original position owing to the restoring force provided by the deformed leg part of the 3D structure, which causes the positive charges in the lower electrode to return to the upper electrode (Figure 2c(iii–v)). The induced charge movement through the series of mechanisms generates the electrical signal. This electrical phenomenon is numerically predicted from the electric potential distribution shown in Figure 2d. Additionally, this simulation result confirms that the positive electric potential at the lower electrode becomes stronger with decreasing t_1.

2.3 | Mechanical Analysis of the 3D Structure With Mechano-Guided Geometrical Adaptation

As discussed in the sensing mechanism of the TUNE sensor, the external force and corresponding electrical output signal of the device are directly related to the displacement of the central part of the 3D structure. In terms of mechanics, the relationship between the force and displacement is associated with the stiffness of the 3D structure. Considering that stiffness, which is the property of a structure to resist deformation under load conditions, is closely related to the sensitivity and working range of a mechanical sensor, exploring the mechanical relationship between force and displacement according to the design parameters of the 3D structure is desirable. However, unlike the general structures, such as beams considered in solid mechanics, the 3D structure used in the TUNE sensor possesses a complex shape, making the general analysis of force and deformation difficult. Therefore, for an intuitive mechanical analysis of complex 3D structures, a dimensional analysis is performed to obtain a qualitative relationship. Figure 3a shows the physical quantities, such as the material properties and sensor dimension parameters, for the mechanical analysis. Here, P is the external force applied to the sensor; u is the displacement of the sensor deformed by P; ε_a is the strain applied to the elastomer substrate after manufacturing the sensor; and L, t, w, and E denote the length, thickness, width, and Young's modulus of the leg part (composed of PI) of the 3D structure, respectively. The basic units of the above physical quantities are as follows: P~[N], ε_a~[1], L~[m], t~[m], w~[m], and E~[N/m^2]. Using the Buckingham π theorem, these physical quantities can be non-dimensionalized by selecting E and L as repeating variables, resulting in the following force–displacement relation in a dimensionless form:

$$\frac{P}{EL^2} = \phi\left(\frac{u}{L}, \varepsilon_a, \frac{t}{L}, \frac{w}{L}\right) \quad (5)$$

where P/EL^2, u/L, t/L, and w/L denote the non-dimensional force, displacement, thickness, and width, respectively. Therefore, the relationship between P/EL^2 and u/L is investigated for the remaining dimensionless variables.

Figure 3b shows the relationship between P/EL^2 and u/L depending on ε_a. In this graph, the slope indicates non-dimensional stiffness of the 3D structure, implying that the 3D structure becomes increasingly compliant to loads as ε_a increases. Therefore, the stiffness of the 3D structure weakens as strain is applied to the elastomer substrate, and the displacement increases for the same load. The behavior of the non-dimensional stiffness (K_{non-d}, slope obtained by linearly fitting the relationship between the data in Figure 3b) of the 3D structure as a function of ε_a is intuitively shown in Figure 3c, with the change of the non-dimensional height (h/L, where h is the height of the 3D structure) of the 3D structure. This result for the height displays the same trend as the numerical simulation analysis in Figure 1c(iii). Considering the mechanism of the TUNE sensor, understanding the factors that indicate the degree to which a structure is likely to be deformed by an external force is helpful. This factor is called compliance and is expressed as the inverse of the stiffness (Figure S4). As shown in Figure 3c,d, the non-dimensional compliance (C_{non-d}) and K_{non-d} exhibit opposite tendencies with ε_a. Furthermore, controlling C_{non-d} by ε_a modulates the critical load that the 3D structure can withstand without collapsing. Here, the critical load is determined by the unique mechanical behavior of the 3D structure. As shown in Figure S5, increasing the displacement of the 3D structure increases and then decreases the load supported by the structure. Since the portion where the load decreases cannot be utilized as a sensor, the maximum resistive load is determined as the critical load (meaning working range). As shown in Figure 3d and Figure S4, the non-dimensional critical force ($P_{c,non-d}$) decreases as ε_a increases. Interestingly, C_{non-d} and $P_{c,non-d}$ have a trade-off relationship, and both are related to the sensitivity and working range of the TUNE sensor. Thus, the stiff 3D structure tolerates relatively severe loading well, whereas the compliant 3D structure is significantly deformed under relatively mild conditions. Therefore, the sensitivity and working range, which are important sensing performances of the sensor, can be adjusted through mechano-guided geometrical adaptation of the 3D structure.

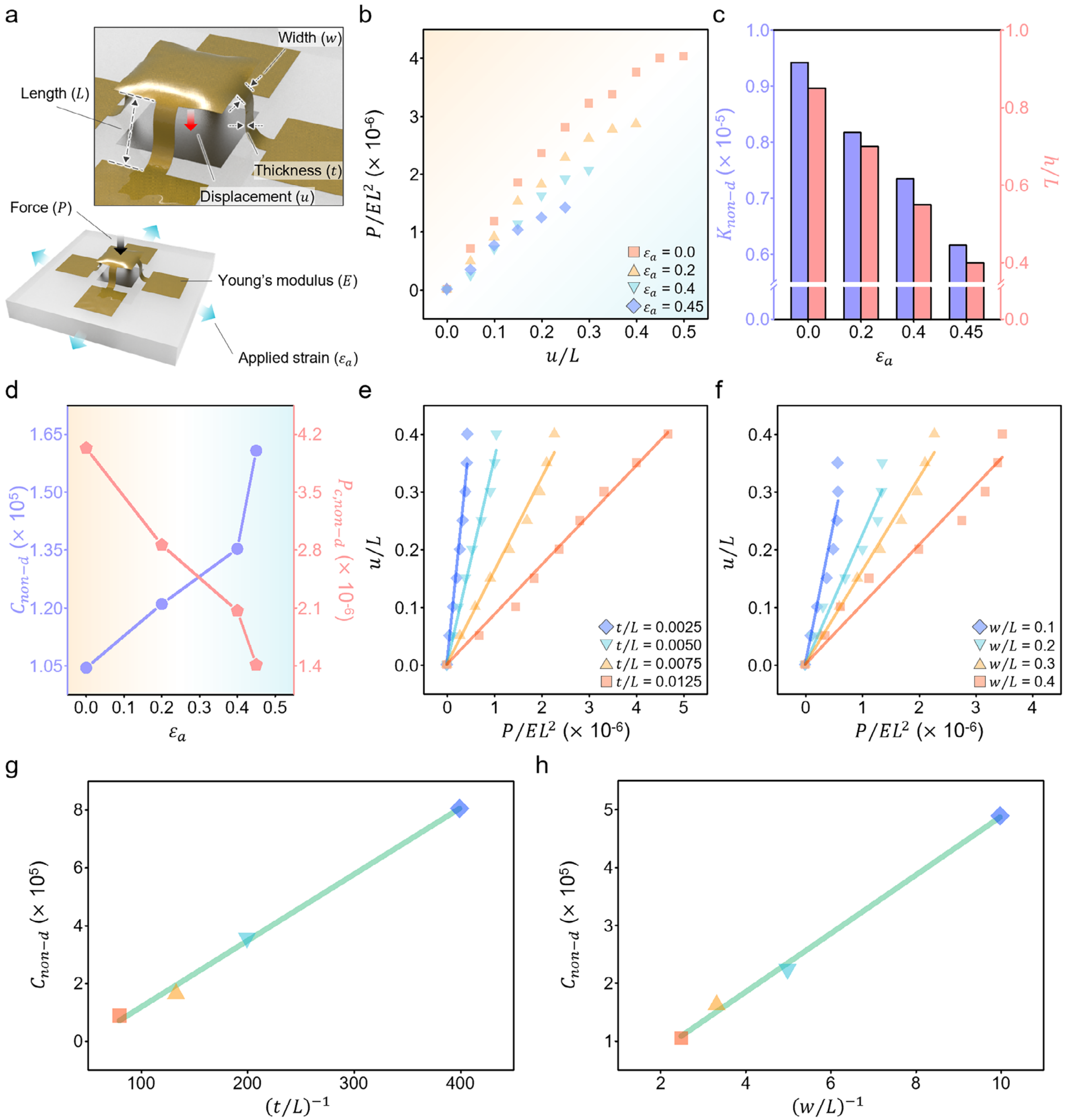

FIGURE 3 | Mechanical analysis of the 3D structure featuring mechano-guided geometrical adaptation. (a) Parameters used in the dimensional analysis of the mechanical response of the 3D structure. (b) Relationship between the non-dimensional force (P/EL^2) and the non-dimensional displacement (u/L) according to the applied strain (ε_a). (c) Non-dimensional stiffness (K_{non-d}) and non-dimensional height (h/L) of the 3D structure according to ε_a. (d) Non-dimensional compliance (C_{non-d}) and non-dimensional critical force ($P_{c,non-d}$) of the 3D structure according to ε_a. C_{non-d} and $P_{c,non-d}$ exhibit a trade-off relationship. (e–f) Relationships between u/L and P/EL^2 according to the non-dimensional thickness (t/L) and the non-dimensional width (w/L). Each solid line represents a linear fit to the corresponding dataset, with all R-squared values exceeding 0.97. (g–h) Effect of dimensionless variables (t/L and w/L) on C_{non-d}. Each solid line represents a linear fit to the corresponding dataset, with all R-squared values exceeding 0.99. The detailed R-squared values corresponding to all linear fits in Figure 3 are provided in Table S1.

The mechanical analysis of the 3D structures for t/L and w/L that can be addressed in the design process is confirmed as shown in Figure 3e,f. The slopes in Figure 3e,f represent C_{non-d}, which exhibits an increasing trend as each dimensionless variable decreases. Thus, stiffening increases with t/L and w/L, and relatively less deformation occurs because of loading. Considering the results in Figure 3d–f, the relationships between C_{non-d} and ε_a, t/L, and w/L can be organized as shown in Figure 3g,h and Figure S6 and expressed as follows:

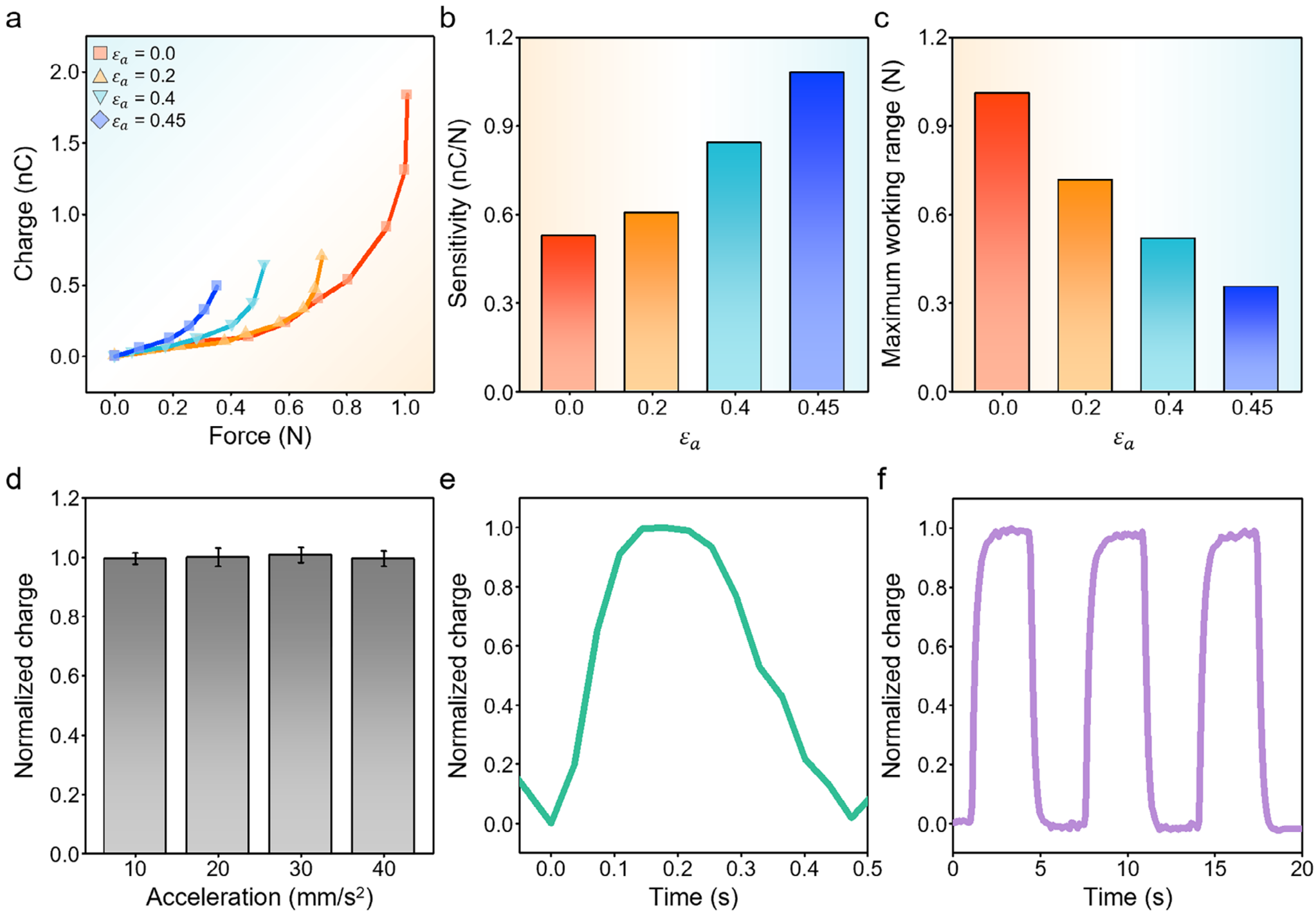

FIGURE 4 | Tunable sensing performance and response characteristics of the TUNE sensor. (a) Output behavior of the TUNE sensor under external force, with respect to ε_a. (b–c) Sensitivity and working range of the TUNE sensor for each ε_a exhibiting a trade-off relationship. (d) Output characteristics of the TUNE sensor under different accelerations of the external force. (e) Response and recovery times of the TUNE sensor. (f) Static sensing characteristics of the TUNE sensor under periodic loading.

$$C_{non-d} \propto \alpha {\varepsilon_a}^{1.3} \left(\frac{t}{L}\right)^{-1} \left(\frac{w}{L}\right)^{-1} \tag{6}$$

where α is the proportional constant. Here, it should be noted that the linear fitting of data about $(t/L)^{-1}$ and $(w/L)^{-1}$ shows a strong linear relationship with R-squared values exceeding 0.99, but the case of ${\varepsilon_a}^{1.3}$ shows a relatively low linear relationship. Nevertheless, this analysis result will help to understand the mechanical behavior of complex 3D structures. The intuitive design guidelines obtained through dimensional analysis can be used to manufacture TUNE sensors suitable for various multivariate environments.

When employing this 3D structure as a sensor, its long-term mechanical stability and fatigue resistance are important factors to consider, as they are closely related to the stress in the structure. The primary deformation of this structure is bending of the leg parts, as shown by the simulation results in Figure S7. From a mechanics-of-materials perspective, the maximum bending stress (σ_{max}) in a leg part is calculated as follows:

$$\sigma_{max} = \frac{M}{I} c \tag{7}$$

where M is the bending moment (related to load), I is the area moment of inertia (related to t and w), and c is the maximum distance from the neutral axis (related to t). Therefore, the stress in the leg parts of the structure is dominated by t and w (related to I and c). Therefore, adjusting these structural parameters to reduce stress can contribute to the long-term stability and fatigue resistance of this sensor.

2.4 | Tunable Sensing Performance and Response Characteristics of the TUNE Sensor

Figure 4 shows the sensing performances of the fabricated TUNE sensor. Figure 4a shows the electrical output transduced from the external force through the TUNE sensor of various ε_a. The TUNE sensor at low ε_a detects a relatively high loading range; however, a more sensitive response occurs as ε_a increases. This result is attributed to compliance control according to ε_a, as confirmed by the mechanical analysis of the buckling-based 3D structure. Interestingly, the nonlinear behavior between the input and output of the TUNE sensor originates from the relationship between the displacement and induced charge, as shown in Equation (3) and Figure 2b. Although the sensor exhibits a nonlinear input–output relationship, it is feasible to utilize different practical applications through electromechanical coupling of the electrostatic-induction mechanism model (Figure 2b) and the mechanical response analysis of the 3D structure (Figure 3). Although the TUNE sensor can successfully control its sensitivity and working range through mechano-guided geometrical adaptation, repeated mechano-guided geometrical adaptation may affect its performance. In this regard, as shown in Figure S8, the behavior of the TUNE sensor before and after 10 cycles of mechano-guided geometrical adaptations is compared. In both states of $\varepsilon_a = 0$ and 0.45, no significant difference is measured between before and after 10 cycles. However, from a practical perspective, repeating more mechano-guided geometrical adaptations may have negative effects due to fatigue of the structure and substrate, so further research from a practical perspective is necessary.

The voltage, current, and power of the TUNE sensor shown in Figure S9 indicate that this sensor converts force into a practical electrical signal. The electricity generated by the TUNE sensor can power a commercial LED device without requiring additional energy (Figure S10). Figure 4b,c show the sensitivity and working range of the sensor as tuned by ε_a; these performance factors correspond to the slope and maximum x-value in Figure 4a, respectively. The results imply that the sensitivity and working range, which can be continuously controlled by ε_a, exhibit a trade-off relationship. In contrast to the simple, dichotomous tunability of sensing performance, either toward high sensitivity or a wide working range, achieved via phase-change materials in previous studies [43–45], the TUNE sensor allows the continuous tuning of performance through a mechanical trigger.

Additionally, the performance related to the dynamic and static responses of the TUNE sensor is investigated. The sensor device outputs a stable electrical signal without being affected by various accelerations under the same load, indicating the excellent dynamic stability of the device output (Figure 4d). In Figure 4e, the response and recovery times of this sensor are 0.14 and 0.22 s, respectively. Notably, the limited sampling rate of our measurement equipment hindered accurate measurements of the response and recovery times. In addition to the dynamic response, the static response of the sensor is an important performance feature that requires investigation. Figure 4f shows the excellent static response of the TUNE sensor for loading-unloading at 3 s intervals.

Furthermore, the electret is a critical element in maintaining a stable sensor signal. According to previous literature on electrets, charges within electrets can escape over time [40, 46]. This charge dissipation depends on the raw material of the electret (Figure S11). The FEP used in this study exhibits the relatively highest initial surface potential and retention rate, but the retention time is short. Environmental factors can also affect electrets. According to existing literature [47], the surface potential of the electret decreases under high temperature and high humidity, and this surface potential is related to the charge injected into the electret. Therefore, improving this environmental impact is important, as the electrostatic signal of the sensor can become unstable under high-temperature and high-humidity environments. According to a previously reported study by our group [48], utilizing an annealing process with the corona charging process can stably maintain charges within the electret under conditions of long time and high humidity. Thus, the fabrication method may allow the TUNE sensor to generate a stable output. In addition to time and humidity, further research is needed to explore the effects of temperature and surface contamination and how this can be reduced.

2.5 | Potential of TUNE Sensor as an Advanced E-Skin

The TUNE sensor, which enables tunable sensitivity and working range through mechano-guided geometrical adaptation, can be applied to advanced forms of e-skin, an application of information and communication technologies, such as the Internet of Things and robotics. A tunable electronic scale using the TUNE sensor is demonstrated representatively to investigate its potential as an advanced e-skin (Figure 5). Figure 5a shows the actual image and performance of the TUNE sensor in the tolerant mode, which has a low sensitivity but a wide working range. The sensitive-mode TUNE sensor, whose sensing performance is opposite to that of the tolerant mode, is realized by applying strain to the elastomer substrate (Figure 5b). Figure 5c,d show the actual deformed shape and corresponding response of the sensor that appear when a mass of 50, 20, 10, or 0.2 g is loaded on the TUNE sensor of each mode. Although the tolerant-mode sensor sufficiently detects a mass of 50 g, owing to the high stiffness of the 3D structure, it does not exhibit a clear response to a load of 0.2 g (Figure 5c). In contrast, a sensitive mode sensor with a highly compliant 3D structure responds to a load of 0.2 g and outputs a high electrical signal for masses of 20 and 10 g. However, owing to the weakness of the 3D structure, the structure collapses at a load of 50 g (Figure 5d). Based on these data, a calibration curve and quantitative model are derived (Figure S12). This demonstration confirms that the mechano-guided geometrical adaptation utilized in the TUNE sensor effectively overcomes the limitations of single-mode sensors with fixed sensing performance.

In practical application scenarios utilizing the TUNE sensor, deciding the approach to control strain is a key point. The pneumatic method of actuating an object using air pressure is suitable for the mechanical triggering method of the TUNE sensor, which is intended for use as an e-skin, due to the lightness of air. Figure 6a shows the TUNE sensor being controlled by air pressure. When air inflation applies strain to the substrate, the TUNE sensor enters sensitive mode. When the air deflates, the TUNE sensor returns to tolerant mode. Figure 6b shows the output of the TUNE sensor in each mode controlled by air pressure. As an application scenario for the TUNE sensor integrated with a pneumatic system, a robotic sensing system for human safety and stable operation is proposed. The pick-and-place process, commonly used in robotic manufacturing, involves the robot picking up a product, moving it to a specific location, and placing it there (Figure 6c). In these robotic environments, collisions between humans and robots can lead to serious accidents. To prevent this, the TUNE sensor can be used for robotic sensing. If a robot equipped with a TUNE sensor in tolerant mode collides with a human, the collision will be detected, but its low sensitivity will cause a

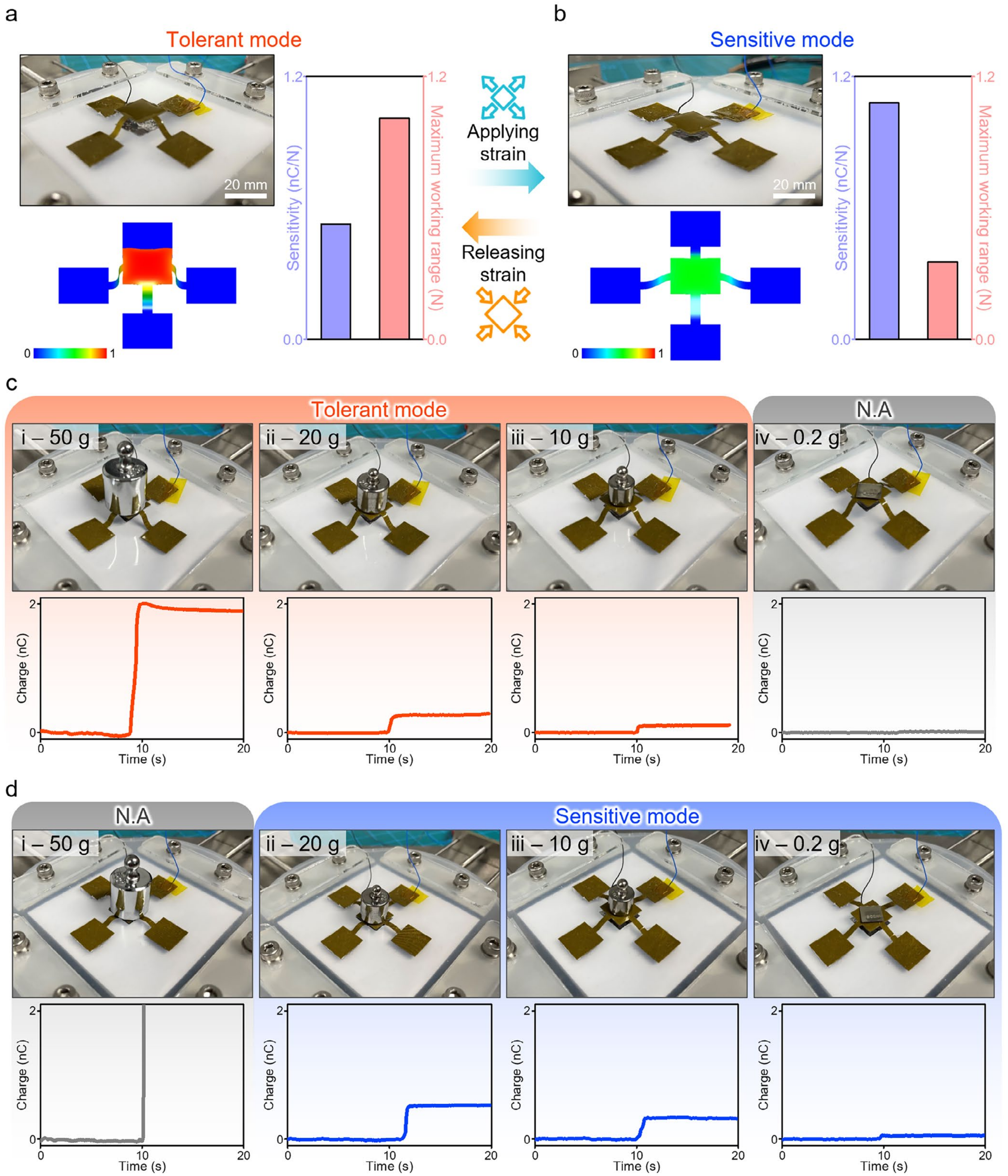

FIGURE 5 | Potential of practical application of the TUNE sensor: Tunable electronic scale. (a–b) Actual images, FEA models, and specifications of the TUNE sensor in tolerant and sensitive modes. (c) Actual image and output signals of the tolerant mode TUNE sensor under various loading conditions. The tolerant mode TUNE sensor shows no response to a 0.2 g load. (d) Actual image and output signals of the sensitive mode TUNE sensor under various loading conditions. The 3D structure of the sensitive mode TUNE sensor collapses under a 50 g load.

slow stop response of the robot, potentially resulting in injury (Figure 6d). In contrast, a TUNE sensor in sensitive mode by air inflation enables rapid robot control through high sensitivity, while the cushioning effect of the air ensures human safety (Figure 6e). Furthermore, to ensure stable operation of the robot in unmanned environments, the sensor can be switched to tolerant mode, preventing it from reacting to any nugacity.

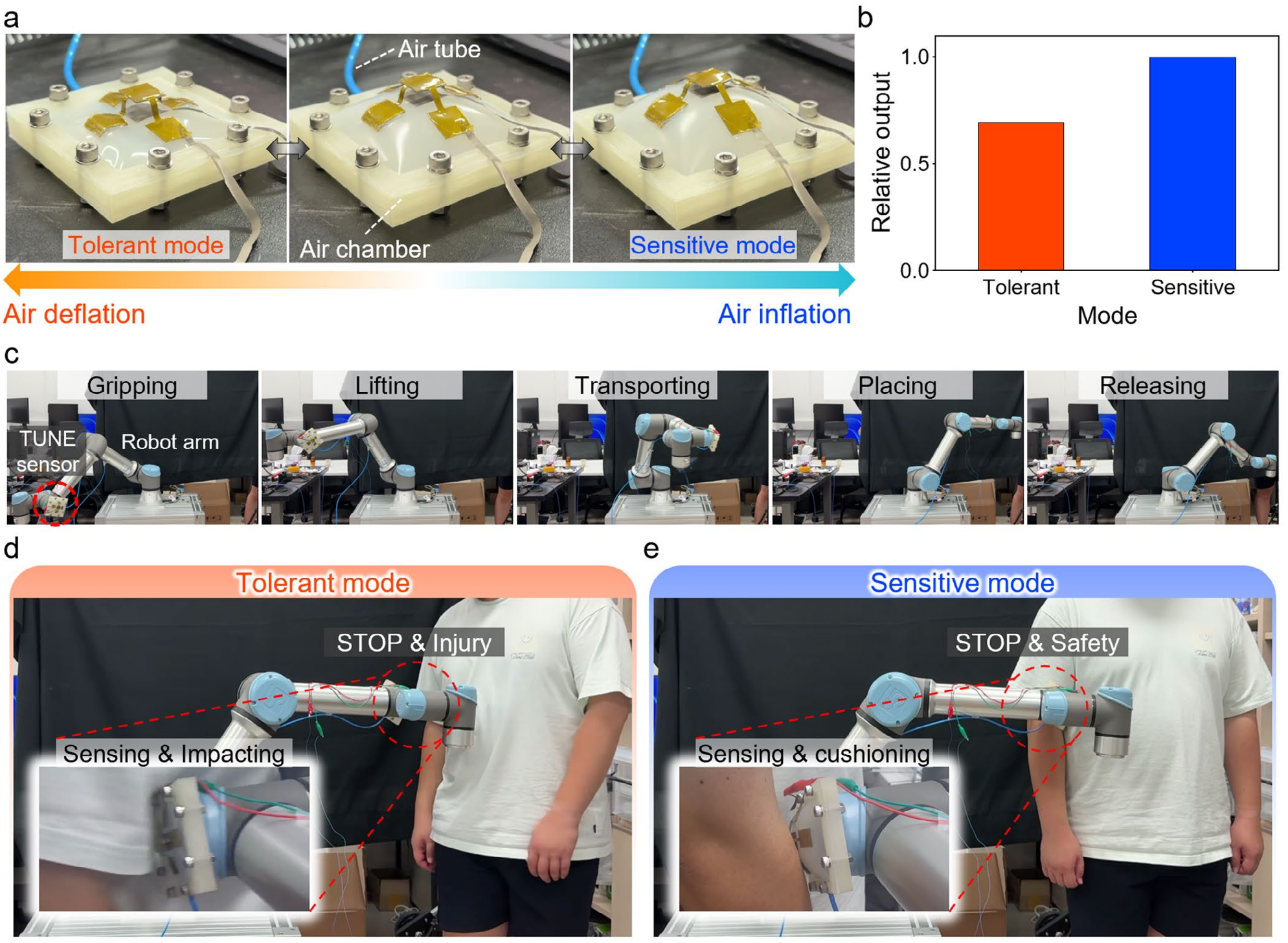

FIGURE 6 | Potential scenario for application of the TUNE sensor: Robotic sensing for human safety and stable operation. (a) TUNE sensor mode controlled by pneumatic pressure. (b) Comparison of the output of the tolerant and sensitive modes of the pneumatically controlled TUNE sensor for the same load. (c) Motion of a robotic arm during the pick and place process. The TUNE sensor is attached to the joint connecting the end of the robot arm and the link. (d) Due to the low sensitivity of the tolerant mode, the robot stops operating after a collision between the robot arm and a human. This poses a risk of injury to humans. (e) In sensitive mode, contact with a human is quickly detected due to high sensitivity. The air cushioning keeps the human safe.

Based on the proposed scenario, latency and signal processing are issues that must be considered for the implementation of the TUNE sensor integrated with a pneumatic system as a practical robotic sensing application. By considering these issues, the process from sensor signal output to robot feedback can be carried out smoothly. Furthermore, multi-directional and dynamic force analysis must be considered because the movements of actual robots are not simple, and a comparison with existing commercial force sensors is necessary. These issues should be addressed in future applied research for the practical application of the proposed scenario, beyond the present basic research.

The strategy of the TUNE sensor, which has shown proof-of-concept as an electronic scale and proposed a potential scenario for robotic sensing, is expected to facilitate the development of advanced e-skin suitable for future intelligent systems.

3 | Conclusion

The TUNE sensor is introduced to overcome the limitations of the fixed detection performance of a single sensor by enabling modulation of the sensitivity of 0.53~1.08 nC/N and working range of 1.01~0.35 N (4.48 to 1.57 kPa as a pressure). The sensing performance of the TUNE sensor is tuned through stiffness control based on mechano-guided geometrical adaptation of its 3D structure. Because tunability is discrete in previous studies that focused on phase change, the proposed approach is distinguished by continuous and reversible performance regulation. Furthermore, the intuitive mechanical understanding of complex 3D structures provides design and utilization guidelines for mechano-guided geometrical adaptation. Adjustment of the sensitivity and working range makes the TUNE sensor suitable for multivariate environments. This novel mechano-guided geometrical adaptation approach offers additional choices in research across application areas such as energy harvesting and actuators, in addition to sensing systems.

The inherent contradiction between the sensitivity and working range of traditional force sensors has been addressed by the TUNE sensor proposed in this study, but a few limitations exist. Compared to previous reports [42, 49], the TUNE sensor has excellent sensitivity but a relatively narrow working range (Figure S9). As shown in Figure S13, because the materials that make up the 2D precursor of a TUNE sensor affect its working range, utilizing composites, shape memory polymers, and gel-based materials may be helpful in sensor performance development of further study. Moreover, this study achieved self-powered conversion of external stimuli into electrical signals, but external energy is still required to control performance. Therefore, future research is expected to integrate energy management/storage circuit technologies and a strain loading system with this TUNE sensor, enabling self-performance control.

4 | Materials and Methods

4.1 | Fabrication of TUNE Sensor Using Mechanically Guided Geometry Transformation

The 2D precursor used to transform to the 3D structure of the TUNE sensor was prepared by blade cutting the layered raw material to which the PI, electrode, and electret were attached to the desired shape using a cutting machine (Silhouette CAMEO4, Silhouette). To apply a compressive force to the 2D precursor, the elastomer substrate (Dragon Skin 20, SMOOTH-ON) was stretched using a custom mechanical stretching system. The prepared 2D precursor was selectively attached to the prestretched substrate using a commercial adhesive. By releasing the prestrain loaded onto the elastomeric substrate, the 2D precursor was transformed into a complex 3D structure, resulting in the TUNE sensor.

The general dimensions of PI used to fabricate the sensor were as follows: $L = 1\,\text{cm}$, $t = t_2 = 75\,\mu\text{m}$, and $w = 3\,\text{mm}$. The electret was square, with dimensions of $1\,\text{cm} \times 1\,\text{cm}$ and a thickness of $t_0 = 250\,\mu\text{m}$. The material properties of PI, namely, E and ε_2, were 2.5 GPa and 3.4, respectively. Additionally, the dielectric constants of FEP (ε) and air (ε_1) were 2.1 and 1.00059, respectively.

4.2 | Electret Fabrication by Corona Charging

The electret was manufactured by artificially injecting electric charges into the dielectric film (FEP) through the corona charging method (Figure S1). The FEP was placed on a grounded plate-type electrode, and a pin-type electrode was placed at a distance of 3 cm. A high voltage of −11 kV was applied to the FEP for 5 min through two electrodes. At this time, the air around the pin-type electrode was ionized, and the ions were artificially inserted into the FEP, resulting in the formation of an electret that semi-permanently formed an electric field around it.

4.3 | Finite Element Analysis for Mechano-Guided Geometrical Adaptation

FEA was conducted using commercial software (SOLIDWORKS) to predict the structural changes of the TUNE sensor resulting from mechano-guided geometrical adaptation. A numerical simulation model was constructed with the same dimensions as the actual sensor. Nonlinear analysis was conducted to account for the large-deformation mechanics of the buckled structure, and a blended curvature-based mesher was adopted. The average element size was 0.657 mm, with a total of 34 157 elements and 60 869 nodes. To obtain a qualitative understanding of the structural behavior, the material properties of PI were applied. Moving boundary conditions at the selective bonding sites in each direction were used to represent applying and releasing strain. The simulation was carried out until the applied strain reached 0.5.

4.4 | Measurement of Mechanical and Electrical Response of TUNE Sensor

To observe the force-displacement mechanical behavior of the TUNE sensor, an electronic scale (HS503, HANSUNG), a custom indentor, and a z-stage were used. The z-stage was used to control the height of the custom indentor, while the electronic scale was used to measure the corresponding force. A specially manufactured pushing tester (JIPT-110, JUNIL TECH, Korea) was used to apply force to the TUNE sensor for electrical response measurements. The electrical output of the TUNE sensor was measured using an electrometer (6514, Keithley).

Author Contributions

Dongik Kam: conceptualization, data curation, formal analysis, investigation, methodology, software, validation, visualization, writing – original draft, and writing – review and editing. **Dayeon Jang:** data curation, formal analysis, investigation, methodology, validation, and writing – original draft. **Hee Jae Hwang:** methodology. **Sunmin Jang:** investigation. **Sumin Cho:** visualization. **Donghan Lee:** investigation. **Donghyeon Yoo:** validation. **Junsang Yoon:** investigation. **Seong Jin Lee:** investigation. **Jongwoo Kim:** resources. **Kyoung Je Cha:** funding acquisition, resources, supervision, and writing – review and editing. **Dongwhi Choi:** conceptualization, funding acquisition, project administration, resources, supervision, validation, and writing – review and editing.

Funding

This work was supported by the Human Resources Development of the Korea Institute of Energy Technology Evaluation and Planning (KETEP) grant funded by the Ministry of Trade, Industry, and Energy of Korea (No. RS-2023-00244330). Additional support was provided by the Ministry of Trade, Industry, and Energy (MOTIE) of Korea through the "Innovative Digital Manufacturing Platform" (Project No. P0022331) supervised by the Korea Institute for Advancement of Technology (KIAT). This work was partially funded by the BK21 FOUR program of the National Research Foundation of Korea (GS-1-JX-NON-20241253).

Conflicts of Interest

The authors declare no conflicts of interest.

References

1. A. T. Rosário and J. C. Dias, "How Industry 4.0 and Sensors Can Leverage Product Design: Opportunities and Challenges," *Sensors* 23, no. 3 (2023): 1165.

2. A. Schütze, N. Helwig, and T. Schneider, "Sensors 4.0–Smart Sensors and Measurement Technology Enable Industry 4.0," *Journal of Sensors and Sensor Systems* 7, no. 1 (2018): 359–371.

3. M. Javaid, A. Haleem, R. P. Singh, S. Rab, and R. Suman, "Significance of Sensors for Industry 4.0: Roles, Capabilities, and Applications," *Sensors International* 2 (2021): 100110.

4. D. Kam, G. Gwon, Y. Ra, et al., "Mechanically Guided 4D Printing of a Triboelectricity-Driven Acoustic Transducer for Self-Powered and Intelligent Voice Recognition," *npj Flexible Electronics* 9, no. 1 (2025): 73.

5. S. Kim, Y. Heo, H. Jung, J. Yoo, J. T. Kim, and Y. Park, "Porous Conductive Composite as Piezoresistive Sensors for Smart Safety Helmet," *Composites Science and Technology* 260 (2025): 110985.

6. J. Kim, E. F. Chou, J. le, S. Wong, M. Chu, and M. Khine, "Soft Wearable Pressure Sensors for Beat-To-Beat Blood Pressure Monitoring," *Advanced Healthcare Materials* 8, no. 13 (2019): 1900109.

7. Y. Park, H. Luan, K. Kwon, et al., "Soft, Full Wheatstone Bridge 3D Pressure Sensors for Cardiovascular Monitoring," *npj Flexible Electronics* 8, no. 1 (2024): 6.

8. J. Y. Oh, D. Son, T. Katsumata, et al., "Stretchable Self-Healable Semiconducting Polymer Film for Active-Matrix Strain-Sensing Array," *Science Advances* 5, no. 11 (2019): eaav3097.

9. J. Kang, D. Son, G. J. N. Wang, et al., "Tough and Water-Insensitive Self-Healing Elastomer for Robust Electronic Skin," *Advanced Materials* 30, no. 13 (2018): 1706846.

10. Y. Lee, S. H. Cha, Y. W. Kim, D. Choi, and J. Y. Sun, "Transparent and Attachable Ionic Communicators Based on Self-Cleanable Triboelectric Nanogenerators," *Nature Communications* 9, no. 1 (2018): 1804.

11. Y. Lee, S. Lim, W. J. Song, et al., "Triboresistive Touch Sensing: Grid-Free Touch-Point Recognition Based on Monolayered Ionic Power Generators," *Advanced Materials* 34, no. 19 (2022): 2108586.

12. D. Kam, G. Gwon, D. Yoo, et al., "Tailoring Dielectric Constant via Anodic Aluminum Oxide-Based Nanoparticle for Boosting the Output Performance of a Triboelectric Nanogenerator," *Chemical Engineering Journal* 500 (2024): 157123.

13. S. S. Rana, O. Faruk, M. S. Reza, M. R. Islam, H. Kim, and J. Y. Park, "All Porous Ecoflex and SEBS-Based Stretchable High-Performance Triboelectric Nanogenerator for Self-Powered Human Activity Monitoring," *Chemical Engineering Journal* 488 (2024): 151050.

14. S. S. Rana, M. T. Rahman, M. A. Zahed, et al., "Zirconium Metal-Organic Framework and Hybridized co-NPC@ MXene Nanocomposite-Coated Fabric for Stretchable, Humidity-Resistant Triboelectric Nanogenerators and Self-Powered Tactile Sensors," *Nano Energy* 104 (2022): 107931.

15. S. S. Rana and Z. L. Wang, "Recent Advances and Prospective Strategies for Improving the Performance of Triboelectric Nanogenerators," *Coordination Chemistry Reviews* 543 (2025): 216914.

16. S. S. Rana, M. A. Zahed, M. R. Islam, et al., "Metal-Organic Framework and Molybdenum Oxide Doped Highly Negative Hybridized Triboelectric Material for Self-Powered and Continuous Monitoring of Biosignals," *Chemical Engineering Journal* 473 (2023): 144989.

17. S. Pyo and K. Park, "Mechanical Metamaterials for Sensor and Actuator Applications," *International Journal of Precision Engineering and Manufacturing-Green Technology* 11, no. 1 (2024): 291–320.

18. J. Qin, L. J. Yin, Y. N. Hao, et al., "Flexible and Stretchable Capacitive Sensors With Different Microstructures," *Advanced Materials* 33, no. 34 (2021): 2008267.

19. S. R. A. Ruth, L. Beker, H. Tran, V. R. Feig, N. Matsuhisa, and Z. Bao, "Rational Design of Capacitive Pressure Sensors Based on Pyramidal Microstructures for Specialized Monitoring of Biosignals," *Advanced Functional Materials* 30, no. 29 (2020): 1903100.

20. S. R. A. Ruth, V. R. Feig, H. Tran, and Z. Bao, "Microengineering Pressure Sensor Active Layers for Improved Performance," *Advanced Functional Materials* 30, no. 39 (2020): 2003491.

21. Y. Luo, M. R. Abidian, J. H. Ahn, et al., "Technology Roadmap for Flexible Sensors," *ACS Nano* 17, no. 6 (2023): 5211–5295.

22. G. Chen, T. Tat, Y. Zhou, et al., "Neural Network-Assisted Personalized Handwriting Analysis for Parkinson's Disease Diagnostics," *Nature Chemical Engineering* 2 (2025): 1–11.

23. X. Zhao, Y. Zhou, W. Kwak, et al., "A Reconfigurable and Conformal Liquid Sensor for Ambulatory Cardiac Monitoring," *Nature Communications* 15, no. 1 (2024): 8492.

24. X. Zhao, Y. Zhou, A. Li, et al., "A Self-Filtering Liquid Acoustic Sensor for Voice Recognition," *Nature Electronics* 7, no. 10 (2024): 924–932.

25. X. Zhao, Y. Zhou, Y. Song, et al., "Permanent Fluidic Magnets for Liquid Bioelectronics," *Nature Materials* 23, no. 5 (2024): 703–710.

26. X. Zhao, Y. Zhou, J. Xu, et al., "Soft Fibers With Magnetoelasticity for Wearable Electronics," *Nature Communications* 12, no. 1 (2021): 6755.

27. Y. Zhou, X. Zhao, J. Xu, et al., "Giant Magnetoelastic Effect in Soft Systems for Bioelectronics," *Nature Materials* 20, no. 12 (2021): 1670–1676.

28. M. Sitti, "Physical Intelligence as a New Paradigm," *Extreme Mechanics Letters* 46 (2021): 101340.

29. H. Kim, J. Choi, K. K. Kim, P. Won, S. Hong, and S. H. Ko, "Biomimetic Chameleon Soft Robot With Artificial Crypsis and Disruptive Coloration Skin," *Nature Communications* 12, no. 1 (2021): 4658.

30. S. Miyashita, "Ingestible, Controllable, and Degradable Origami Robot for Patching Stomach Wounds," in *2016 IEEE International Conference on Robotics and Automation (ICRA)* (IEEE, 2016).

31. M. Han, H. Wang, Y. Yang, et al., "Three-Dimensional Piezoelectric Polymer Microsystems for Vibrational Energy Harvesting, Robotic Interfaces and Biomedical Implants," *Nature Electronics* 2, no. 1 (2019): 26–35.

32. D. Kam, H. Choi, G. Gwon, et al., "Toward Droplet Energy Harvesting in Harsh Environment: Mechanical Buckling-Induced 3D Structured Droplet-Based Electricity Multigenerator," *Small* 21 (2025): 2502717.

33. D. Kam, G. Gwon, S. Jang, et al., "Advancing Energy Harvesting Efficiency From a Single Droplet: A Mechanically Guided 4D Printed Elastic Hybrid Droplet-Based Electricity Generator," *Advanced Materials* 35, no. 48 (2023): 2303681.

34. D. Kam, S. Oh, J.-G. Kim, and D. Choi, "Mechanical Buckling Assisted Formation of 3D Conductive Composite Meso-Structure for Highly Sensitive Piezoresistive Pressure Sensor," *Composite Structures* 311 (2023): 116808.

35. B. H. Kim, K. Li, J. T. Kim, et al., "Three-Dimensional Electronic Microfliers Inspired by Wind-Dispersed Seeds," *Nature* 597, no. 7877 (2021): 503–510.

36. H. Luan, Q. Zhang, T. L. Liu, et al., "Complex 3D Microfluidic Architectures Formed by Mechanically Guided Compressive Buckling," *Science Advances* 7, no. 43 (2021): eabj3686.

37. X. Ning, X. Wang, Y. Zhang, et al., "Assembly of Advanced Materials Into 3D Functional Structures by Methods Inspired by Origami and Kirigami: A Review," *Advanced Materials Interfaces* 5, no. 13 (2018): 1800284.

38. X. Wang, X. Guo, J. Ye, et al., "Freestanding 3D Mesostructures, Functional Devices, and Shape-Programmable Systems Based on Mechanically Induced Assembly With Shape Memory Polymers," *Advanced Materials* 31, no. 2 (2019): 1805615.

39. S. M. Won, H. Wang, B. H. Kim, et al., “Multimodal Sensing With a Three-Dimensional Piezoresistive Structure,” *ACS Nano* 13, no. 10 (2019): 10972–10979.

40. M. G. Broadhurst, G. T. Davis, R. Gerhard-Multhaupt, et al., *Electrets*, vol. 33 (Springer Science & Business Media, 2005).

41. S. Gong, C. Wang, J. Zhang, C. Zhang, J. E. West, and K. Ren, “Monocharged Electret Generator for Wearable Energy Harvesting Applications,” *Advanced Sustainable Systems* 2, no. 5 (2018): 1700178.

42. S. Gong, J. Zhang, C. Wang, K. Ren, and Z. L. Wang, “A Monocharged Electret Nanogenerator-Based Self-Powered Device for Pressure and Tactile Sensor Applications,” *Advanced Functional Materials* 29, no. 41 (2019): 1807618.

43. S.-H. Byun, J. Y. Sim, Z. Zhou, et al., “Mechanically Transformative Electronics, Sensors, and Implantable Devices,” *Science Advances* 5, no. 11 (2019): eaay0418.

44. H. Jing, L. Xu, X. Wang, Y. Liu, and J. Hao, “A Phase-Change Gel Based Pressure Sensor With Tunable Sensitivity for Artificial Tactile Feedback Systems,” *Journal of Materials Chemistry A* 9, no. 35 (2021): 19914–19921.

45. S. Lee, S. H. Byun, C. Y. Kim, et al., “Beyond Human Touch Perception: An Adaptive Robotic Skin Based on Gallium Microgranules for Pressure Sensory Augmentation,” *Advanced Materials* 34, no. 44 (2022): 2204805.

46. A. Thyssen, *Charge Distribution and Stability in Electret Materials* (DTU Nanotech, 2016).

47. C. Liu, Z. Dai, B. He, and Q. F. Ke, “The Effect of Temperature and Humidity on the Filtration Performance of Electret Melt-Blown Nonwovens,” *Materials* 13, no. 21 (2020): 4774.

48. Y. Yun, M. La, S. Cho, et al., “High Quality Electret Based Triboelectric Nanogenerator for Boosted and Reliable Electrical Output Performance,” *International Journal of Precision Engineering and Manufacturing-Green Technology* 8, no. 1 (2021): 125–137.

49. K. Parida, V. Bhavanasi, V. Kumar, R. Bendi, and P. S. Lee, “Self-Powered Pressure Sensor for Ultra-Wide Range Pressure Detection,” *Nano Research* 10, no. 10 (2017): 3557–3570.

Supporting Information

Additional supporting information can be found online in the Supporting Information section. **Figure S1:** Electret fabrication and the electric field generated by the electret. (a) Corona charging system used for electret fabrication. (b) Schematic illustration of the electric field generated by the electret. **Figure S2:** Decomposition of force applied to the 3D structure of the TUNE sensor. θ_s and θ_c denote the angle between the leg of the 3D structure and the ground in the stiff and compliant structures, respectively. Within the strain region considered in this work, the angle between the leg of the 3D structure and the ground varies from 0° to 90°. **Figure S3:** Surface potential of electrets according to raw materials. **Figure S4:** Relationship between the non-dimensional displacement (u/L) and the non-dimensional force (P/EL^2) according to the applied strain (ε_a). (a) $\varepsilon_a = 0.0$. (b) $\varepsilon_a = 0.2$. (c) $\varepsilon_a = 0.4$. (d) $\varepsilon_a = 0.45$. The slope and maximum x-value in each graph correspond to the non-dimensional compliance (C_{non-d}) and the non-dimensional critical force ($P_{c,non-d}$), respectively. **Figure S5:** Interesting mechanical behavior of 3D structure used to TUNE sensor. As the displacement of the 3D structure increases, the force supported by the structure increases and then decreases. The working range of the sensor is selected to be the maximum force that does not cause the structure to collapse. **Figure S6:** Effect of dimensionless variable ε_a on C_{non-d}. The solid line represents a linear fit to the corresponding dataset. The R-squared value is 0.88. **Figure S7:** Von Mises stress distribution within the 3D structure of the TUNE sensor. Most of the large stress is concentrated in the leg part, which is attributed to bending. **Figure S8:** Behavior of the TUNE sensor before and after 10 cycles of mechano-guided geometrical adaptation. (a) TUNE sensor with $\varepsilon_a = 0$. (b) TUNE sensor with $\varepsilon_a = 0.45$. **Figure S9:** Various electrical outputs of the TUNE sensor ($\varepsilon_a = 0.45$). (a) Voltage depending on force. The sensitivity is 4.66 V/N (= 1.05 V/kPa). (b) Current depending on force. (c) Power depending on force. **Figure S10:** Demonstration of powering an LED from electricity generated by applying a force on the TUNE sensor. (a) Setup. The TUNE sensor and LED are directly connected without any additional electronic components. LED off during non-loading force. (b) LED on when loading force. **Figure S11:** Charge stability of electrets depending on raw material. **Figure S12:** Calibration curve and quantitative model of the electronic scale application. This result is obtained through data in tolerant mode and has an R-squared value of 0.97. **Figure S13:** Force sensing behavior of a TUNE sensor fabricated with PLA instead of PI ($\varepsilon_a = 0.0$). The PLA-based sensor has a 150% improved working range compared to the PI-based sensor. The Young's modulus of PLA is 3.2 GPa. **Table S1:** The detailed R-squared values corresponding to all linear fits in Figure 3.